HHS Public Access

Author manuscript

*Cell Rep*. Author manuscript; available in PMC 2016 January 28.

Published in final edited form as:

*Cell Rep*. 2016 January 26; 14(3): 403–410. doi:10.1016/j.celrep.2015.12.054.

# EMRE is a Matrix $Ca^{2+}$ Sensor that Governs Gatekeeping of the Mitochondrial $Ca^{2+}$ Uniporter

**Horia Vais**[1,#], **Karthik Mallilankaraman**[1,2,#], **Don-On Daniel Mak**[1], **Henry Hoff**[1], **Riley Payne**[1], **Jessica Tanis**[1], and **J. Kevin Foskett**[1,3,*]

[1]Department of Physiology, Perelman School of Medicine, University of Pennsylvania, Philadelphia, PA, USA

[3]Department of Cell and Developmental Biology, Perelman School of Medicine, University of Pennsylvania, Philadelphia, PA, USA

## SUMMARY

The mitochondrial uniporter (MCU) is an ion channel that mediates $Ca^{2+}$ uptake into the matrix to regulate metabolism, cell death and cytoplasmic $Ca^{2+}$ signaling. Matrix $Ca^{2+}$ concentration is similar to that in cytoplasm, despite an enormous driving force for entry, but the mechanisms that prevent mitochondrial $Ca^{2+}$ overload are unclear. Here, we show that MCU channel activity is governed by matrix $Ca^{2+}$ concentration through EMRE. Deletion or charge neutralization of its matrix-localized acidic carboxyl terminus abolishes matrix $Ca^{2+}$ inhibition of MCU $Ca^{2+}$ currents, resulting in MCU channel activation, enhanced mitochondrial $Ca^{2+}$ uptake and constitutively elevated matrix $Ca^{2+}$ concentration. EMRE-dependent regulation of MCU channel activity requires intermembrane space-localized MICU1, MICU2 and cytoplasmic $Ca^{2+}$. Thus, mitochondria are protected from $Ca^{2+}$ depletion and $Ca^{2+}$ overload by a unique molecular complex that involves $Ca^{2+}$ sensors on both sides of the inner mitochondrial membrane, coupled through EMRE.

## INTRODUCTION

The mitochondrial calcium uniporter is a $Ca^{2+}$-selective ion channel localized in the inner mitochondrial membrane (IMM) (Gunter et al., 1994; Kirichok et al., 2004) that mediates $Ca^{2+}$ uptake into the mitochondrial matrix from the cytoplasm to regulate metabolism, cell death and cytoplasmic $Ca^{2+}$ signaling. Under normal resting conditions the matrix free $Ca^{2+}$

*Corresponding author: J. Kevin Foskett, 700 Clinical Research Building/6085, University of Pennsylvania, Philadelphia, PA 19104-6085, Phone: (215) 898-1354, foskett@mail.med.upenn.edu.

[2]current address: Mitochondrial Physiology and Metabolism Lab, Department of Physiology, Yong Loo Lin School of Medicine, National University of Singapore, Singapore 117597

[#]These authors contributed equally to this work

**AUTHOR CONTRIBUTIONS**

H.V. performed the electrophysiology. K.M. performed permeabilized cell experiments, made cell lines and created cDNA constructs. D-O.D.M helped analyze data. R.P. performed Rhod-2 imaging and some permeabilized cell experiments. J.T. and H.H. performed biochemistry. J.K.F, H.V., K.M. J.T. and D-O.D.M wrote the manuscript. The authors declare no competing financial interests.

concentration is similar to that in the cytoplasm (Lukacs and Kapus, 1987; Nicholls, 2009), despite an enormous ~180 mV driving force for $Ca^{2+}$ entry generated by proton pumping by the respiratory chain, suggesting that the $Ca^{2+}$ uniporter possesses mechanisms to inactivate it under resting conditions to prevent mitochondrial $Ca^{2+}$ overload. However, the nature of such mechanisms is unclear. The mitochondrial $Ca^{2+}$ uniporter is a complex of proteins including the $Ca^{2+}$ selective pore-forming subunit MCU and accessory proteins including MICU1, MICU2, MCUR1 and EMRE (De Stefani and Rizzuto, 2014; Foskett and Philipson, 2015; Kamer et al., 2014). Previously it was suggested that either MICU1 or MICU2 provided a so-called gatekeeping function that reduces MCU-mediated $Ca^{2+}$ uptake *in situ* below a threshold value of 1–2 μM external free $Ca^{2+}$ (the low cytoplasmic [$Ca^{2+}$] regime) to prevent mitochondrial $Ca^{2+}$ loading under basal conditions (Csordas et al., 2013; Mallilankaraman et al., 2012; Patron et al., 2014), most likely by reducing MCU single channel open probability. However, it is unclear if MICU proteins exert their effects from the matrix or inter-membrane space or if $Ca^{2+}$ binding to their pairs of EF hands is required (Foskett and Madesh, 2014). Furthermore, their regulation of MCU-mediated $Ca^{2+}$ uptake has not been examined by electrophysiological studies of the uniporter channel directly in its native membrane environment, so the molecular details of channel regulation by MICU1 and MICU2 remain unknown. The importance of understanding this regulatory mechanism is underscored by patients with loss of function mutations in MICU1, who lack inhibition of mitochondrial $Ca^{2+}$ uptake under basal conditions and exhibit proximal myopathy, learning difficulties and a progressive extrapyramidal movement disorder (Logan et al., 2014).

## RESULTS

We recorded uniporter $Ca^{2+}$ currents ($I_{MiCa}$) using patch clamp electrophysiology of mitoplasts (Fieni et al., 2012; Kirichok et al., 2004; Vais et al., 2015) isolated from human embryonic kidney (HEK) cells. In the whole-mitoplast recording configuration with the pipette solution lacking $Ca^{2+}$, ruthenium red (RuR, 200 nM)-sensitive $Ca^{2+}$ currents were observed (Figure 1A) with densities and properties similar to those previously reported for $I_{MiCa}$ with matrix [$Ca^{2+}$] buffered either at zero or >10 μM (Fieni et al., 2012; Kirichok et al., 2004). Similar currents were nearly abolished in cells with MCU knocked down (Figure 1B), confirming their identity as uniporter currents. Unexpectedly, $I_{MiCa}$ was markedly reduced when matrix [$Ca^{2+}$] was raised from 0 into a range from 30 nM to ~400 nM (Figure 1C), resulting in a biphasic matrix [$Ca^{2+}$] dependence with apparent inhibition constant of 60 ± 30 nM and Hill coefficient of 1.0 ± 0.2, and apparent recovery constant of 730 ± 15 nM and Hill coefficient of 3.1 ± 1.6, with peak inhibition of MCU currents by ~75% at ~400 nM (Figure 1D). Of note, resting matrix [$Ca^{2+}$] is ~100–300 nM (Boyman et al., 2014; Brandenburger et al., 1996; Ivannikov and Macleod, 2013; Lukacs and Kapus, 1987; Nicholls, 2009; Palmer et al., 2006), suggesting that this inhibition of MCU activity may be related to the previously reported inhibition of MCU activity in the low $Ca^{2+}$ regime attributed to MICU1 and MICU2.

Using a proteinase sensitivity assay (Sato and Mihara, 2010), we determined that MICU1 and MICU2 are localized outside of the matrix, in the intermembrane space (IMS; Figure S1A), in agreement with other reports (Csordas et al., 2013; Kamer and Mootha, 2014; Lam et al., 2015; Petrungaro et al., 2015; Sancak et al., 2013). This suggested that matrix [$Ca^{2+}$]

regulation of $I_{MiCa}$ is mediated by MCU itself or by another matrix-localized $Ca^{2+}$ binding protein. Plasma membrane $Ca^{2+}$ channels also have $Ca^{2+}$ dependent channel inactivation, usually mediated by an associated protein (Christel and Lee, 2012). EMRE is a single pass 10 kD IMM protein that binds to MCU and is required for uniporter activity (Sancak et al., 2013), although its function is unknown. By protease sensitivity biochemistry, we determined that the carboxyl terminus of EMRE faces into the mitochondrial matrix (Figure 2A and Figure S1B). The carboxyl terminus contains a conserved acidic motif that is homologous to the $Ca^{2+}$ binding "$Ca^{2+}$ bowl" and "$Ca^{2+}$ clasp" in $Ca^{2+}$-activated large conductance (BK) $K^+$ and bestrophin $Cl^-$ channels, respectively (Figure S1C). We speculated that it similarly bound $Ca^{2+}$ in EMRE. Deletion of the EMRE carboxyl terminus or charge neutralization of its seven terminal acidic residues (Figure S1C) was without effect on MICU1 or MICU2 localization (Figure S1D), EMRE topology (Figure S1D and S1E), expression of MCU, MICU1 or MICU2 (Figure S2C) or ability of EMRE to interact with MCU (Figure S3) but it abolished matrix $[Ca^{2+}]$ regulation of uniporter $Ca^{2+}$ currents (Figure 2B–F). Loss of matrix $[Ca^{2+}]$ inhibition of MCU channel activity in mutant EMRE-expressing cells resulted in constitutively elevated matrix $[Ca^{2+}]$ (Figure 2G–L and Figure S4).

To determine the relationship between these observations and previously reported regulation of MCU activity by MICU1 and MICU2, we examined MCU activity in intact mitochondria by simultaneous measurements of mitochondrial $Ca^{2+}$ uptake and mitochondrial membrane potential in permeabilized HEK293 cells as previously described (Mallilankaraman et al., 2012). Addition of digitonin to permeabilize the plasma membrane and thapsigargin to inhibit SERCA activity slowly raised bath $[Ca^{2+}]$ due to leak of $Ca^{2+}$ from the endoplasmic reticulum (ER). Addition of CGP37157 (CGP) to inhibit the IMM $Na^+/Ca^{2+}$ exchanger and reveal the rate of unidirectional mitochondrial $Ca^{2+}$ uptake, reversed that trend for all cells with functional MCU (Figure 2M and 2N). In contrast, the slow rise in bath $[Ca^{2+}]$ was unaffected by CGP addition in EMRE-KO cells (Figure 2N), reflecting absence of mitochondrial $Ca^{2+}$ uptake, as expected since EMRE KO abrogates MCU activity in HEK293 cells (Sancak et al., 2013). In response to addition of a 10 μM $Ca^{2+}$ bolus, bath $[Ca^{2+}]$ was rapidly reduced by MCU-mediated $Ca^{2+}$ uptake in WT cells, whereas it remained high with no reduction in EMRE-KO cells (Figure 2N), confirming that EMRE is critical for MCU $Ca^{2+}$ channel function. Control experiments showed complete abrogation of $I_{MiCa}$ in EMRE-KO cells (n = 6; data not shown). MCU-mediated $Ca^{2+}$ uptake in response to addition of a 10 μM $Ca^{2+}$ bolus was restored in EMRE-rescue cells (Figure 2N) and in cells rescued with carboxyl-terminus mutant EMRE (Figure 2M). Unidirectional $Ca^{2+}$ uptake through MCU observed after CGP addition (Figure 2M and N) reduced bath $[Ca^{2+}]$ for WT cells to a significantly higher level than that for mutant EMRE cells, indicating that inhibition of MCU activity in the low cytoplasmic $[Ca^{2+}]$ regime that terminated $Ca^{2+}$ uptake in WT cells was lost in cells expressing mutant EMRE. Even in the absence of $Na^+/Ca^{2+}$ exchanger activity in WT cells, no decrease in bath $[Ca^{2+}]$ was detected after the addition of a 0.5 μM $Ca^{2+}$ bolus, (Figure 2N), whereas bath $[Ca^{2+}]$ was restored to the pre-$Ca^{2+}$ addition level after the addition of 0.5 μM $Ca^{2+}$ to carboxyl-terminus mutant EMRE cells (Figure 2N), suggesting also that normal inhibition of MCU activity in the low cytoplasmic $[Ca^{2+}]$ regime was impaired by EMRE carboxyl terminus charge neutralization

or deletion. These results indicate that EMRE is a $Ca^{2+}$ sensor that mediates matrix [$Ca^{2+}$] regulation of uniporter activity.

It was originally reported that MICU1 conferred inhibition of MCU-mediated mitochondrial $Ca^{2+}$ influx in the low cytoplasmic [$Ca^{2+}$] regime (Mallilankaraman et al., 2012). It was subsequently suggested that MICU2 instead mediates this inhibition of MCU activity (Patron et al., 2014). Measurements of mitochondrial $Ca^{2+}$ uptake in permeabilized cells confirmed that knockout of either MICU1 or MICU2 abrogated normal inhibition of MCU activity in the low cytoplasmic [$Ca^{2+}$] regime (Figure 3A), resulting in constitutive matrix $Ca^{2+}$ loading (Figure 3B–D and Figure S4). To explore the relationship between the EMRE-dependent matrix [$Ca^{2+}$] regulation of $I_{MiCa}$ and apparent inhibitory functions of MICU proteins, we recorded $I_{MiCa}$ in cells with either MICU protein knocked down. Remarkably, knockdown or knockout of either MICU1 or MICU2 (Figure S2A and 2B) abolished matrix [$Ca^{2+}$] regulation of $I_{MiCa}$ (Figure 3E and 3F). $I_{MiCa}$ regulation (Figure 3E and 3F) and constitutive mitochondrial $Ca^{2+}$ loading (Figure 3B and 3C) were rescued by expression of the wild-type proteins (Figure 3F and 3H–L). These results indicate that matrix [$Ca^{2+}$] regulation of $I_{MiCa}$ is part of the so-called gatekeeping mechanism underlying previously reported inhibition of MCU activity in the low cytoplasmic [$Ca^{2+}$] regime.

It was suggested that MICU1- (Csordas et al., 2013) or MICU2- (Patron et al., 2014) mediated inhibition of MCU activity does not require $Ca^{2+}$ binding to their EF hands. To explore the role of cytoplasmic $Ca^{2+}$ in EMRE regulation of MCU activity, we removed $Ca^{2+}$ from the bath and recorded MCU activity by measuring $Na^{+}$ currents (Figure 4A–C) (Fieni et al., 2012; Kirichok et al., 2004). Normal matrix [$Ca^{2+}$] (400 nM) inhibition of MCU activity was eliminated in the absence of bath $Ca^{2+}$ (Figure 4A–C), suggesting that $Ca^{2+}$ binding in the intermembrane space, perhaps to MICU1 and/or MICU2 or MCU itself, is required for EMRE-dependent matrix [$Ca^{2+}$] regulation of $I_{MiCa}$. It has been suggested that MICU2 suppresses MCU activity (Patron et al., 2014). However, comparable $Na^{+}$ currents were recorded in MICU2 KO cells (Figure 4C).

## DISCUSSION

Our results suggest a novel model employing $Ca^{2+}$ sensors on both sides of the IMM in which the activity of the mitochondrial uniporter is tuned to provide optimal $Ca^{2+}$ influx into the mitochondrial matrix under resting conditions. EMRE is a sensor of matrix [$Ca^{2+}$] that governs the inhibition of uniporter activity under normal conditions, acting to prevent mitochondrial $Ca^{2+}$ loading under basal conditions. This function requires conserved acidic residues in the matrix-localized carboxyl tail of EMRE as well as MICU1 and MICU2 and $Ca^{2+}$ on the opposite side of the IMM (Figures 4D and S4B). Of note, EMRE mediates the interaction of MICU proteins with MCU (Sancak et al., 2013), suggesting a possible mechanism for EMRE and MICU proteins to have coupled functions. EMRE-dependent matrix [$Ca^{2+}$] regulation of $I_{MiCa}$ may also play a role in preventing mitochondrial $Ca^{2+}$ depletion when cytoplasmic [$Ca^{2+}$] becomes low or mitochondrial $Ca^{2+}$ extrusion exceeds influx (Figure 4D and S4B). Under such conditions, $Ca^{2+}$ may dissociate from EMRE and possibly MICU proteins, relieving inhibition of MCU and enabling uniporter activity to increase to preserve matrix [$Ca^{2+}$] to support critical mitochondrial functions (Cardenas et

al., 2010). Thus, mitochondria are protected both from $Ca^{2+}$ depletion under low-$Ca^{2+}$ conditions and from $Ca^{2+}$ loading under normal resting conditions by a unique molecular complex that involves $Ca^{2+}$ sensors on both sides of the IMM, governed by EMRE. Our results suggest a model in which agonist-generated cytoplasmic $Ca^{2+}$ signals raise matrix [$Ca^{2+}$] due to the non-zero open probability of MCU under basal conditions, to a level (> 1 μM; Figure 1D that relieves EMRE-mediated matrix [$Ca^{2+}$] inhibition of uniporter activity (Figures 1D, 4D, and S4B), enabling agonist-activated cytoplasmic $Ca^{2+}$ signals to be conveyed to the matrix to stimulate respiration. The mechanism of matrix [$Ca^{2+}$]-mediated relief from inhibition is highly cooperative (apparent Hill coefficient ~3, Figure 1D) and may therefore account for observed cooperative $Ca^{2+}$ activation of the uniporter (Bragadin et al., 1979; Gunter and Pfeiffer, 1990; Zoccarato and Nicholls, 1982) without the need to invoke amplification by $Ca^{2+}$ binding to MICU1 (Csordas et al., 2013; Perocchi et al., 2010). Importantly, the nature of the mechanism(s) involved in matrix [$Ca^{2+}$] activation of the uniporter remain to be determined (Figure 4D and S4B).

## EXPERIMENTAL PROCEDURES

### Cell lines and constructs

Wild-type HEK-293T, MICU1-KO, MICU2-KO and EMRE-KO cell lines were grown in Dulbecco's modified Eagle's medium (DMEM) supplemented with 10% FBS, 100 U/ml penicillin, and 100 μg/ml streptomycin at 37 °C and 5% $CO_2$. All knockout (KO) cell lines were gifts from Dr. Vamsi Mootha. MICU1 knockdown (KD) cells were generated by lentiviral transduction of shRNAs targeting MICU1; transduced cells were selected and maintained in complete DMEM supplemented with puromycin (2 μg/ml), as described (Mallilankaraman et al., 2012). Full length MICU1, MICU2 and EMRE cDNAs were purchased from Origene Technologies USA. EMRE-ΔC-V5 and EMRE-QN6-V5 constructs were generated by a PCR-based cloning strategy. All constructs were sequence verified and stably transfected into either KD or KO backgrounds.

### Uniporter electrophysiology

Mitoplast electrophysiology was performed as described (Fieni et al., 2012; Kirichok et al., 2004; Vais et al., 2015). For $I_{MiCa}$ measurements, patch pipettes with tip diameters significantly less than 1 μm had resistances of 20 – 60 MΩ when filled with (in mM): TMA-OH, 130 mM; Hepes, 100; glutathione, 10; $MgCl_2$, 2; EGTA, 1.5; pH = 7.0 with D-gluconic acid; osmolarity 330–350 mOsm/kg. EGTA was also used to buffer different amounts of $CaCl_2$, for $[Ca^{2+}]_{free} \leq 600$ nM. However, EGTA was replaced by 1.5 mM of: dibromo-Bapta (for 600 nM < $[Ca^{2+}]_{free} \leq 4$ μM), HEDTA (for 4 μM ≤ $[Ca^{2+}]_{free} \leq 30$ μM), or NTA (for $[Ca^{2+}]_{free} = 100$ μM). In all pipette solutions, $[Ca^{2+}]_{free}$ (< 100 μM) was confirmed by $Ca^{2+}$-indicator dye fluorimetry. For $Na^+$ current measurements, pipettes were filled with (in mM): Na-gluconate, 110; Hepes, 40; NaCl, 2; EGTA, 1; EDTA, 5; $CaCl_2$, see above; pH = 7.0 with NaOH; osmolarity 330–350 mOsm/kg. Mitoplasts were initially bathed in (in mM): KCl, 150; Hepes, 10; EGTA, 1; pH = 7.2, osmolarity 300 mOsm/Kg ("KCl-DVF" solution). Voltage pulses of 350 – 500 mV amplitude and 15 – 50 ms duration, delivered by the PClamp-10 (Molecular Devices) program, were used to obtain the "whole-mitoplast" configuration. Access resistance (30 – 90 MΩ) and mitoplast capacitance $C_m$ (0.2 – 1 pF)

were determined using the membrane test protocol of the PClamp-10 software. Because the volume of a mitoplast is over three orders of magnitude smaller than that of a cell, we assumed that matrix $[Ca^{2+}]_{free}$ rapidly equilibrated with pipette $[Ca^{2+}]_{free}$. After the whole-mitoplast configuration was obtained, the KCl-DVF bath solution was exchanged with: Hepes-EGTA [(in mM): Hepes, 150; EGTA, 1.5; pH = 7.0 with Tris-base for baseline (control) measurements, followed by Hepes (no EGTA) solutions with 0.1; 0.3; 1 mM $CaCl_2$, successively. Finally, a Hepes-based solution with 1 mM $CaCl_2$ and 200 nM ruthenium red (RuR) was perfused into the bath to record the final baseline (= $I_{RuR}$) after block of MCU $Ca^{2+}$ currents. For MCU $Na^+$ current measurements, the Hepes-EGTA control solution was instead exchanged with (in mM): Na-gluconate 110; Hepes, 40; EGTA, 1; EDTA, 5; pH = 7.0, followed by the same solution supplemented with 4 mM $CaCl_2$ ($[Ca^{2+}]_f \approx 180$ nM, estimated with the MaxChelator software), to block the $Na^+$ currents. Osmolarities of all bath solutions were 297–305 mOsm/Kg, adjusted with sucrose. The voltage protocol, delivered by the PClamp-10 software with a DigiData-1550 interface (Molecular Devices), consisted of stepping from $V_m$ = 0 mV to -160 mV for 20 ms, followed by ramping to 80 mV (rate of 279 mV/s), dwelling at 80 mV for 20 ms and return to 0 mV. Currents were recorded using an Axopatch 200-B amplifier. Data were acquired at room temperature with a sampling rate of 50 kHz and anti-aliasing filtered at 1 kHz. Data analysis was performed with the PClamp-10 software. For quantitative comparisons, current densities defined as:

$$I_{MCU}/C_m = (I_{Ca} - I_{RuR})/C_m$$

with $I_{Ca}$ and $I_{RuR}$ measured at $V_m$ = −160 mV in the presence of 1 mM $Ca^{2+}$ in the bath, were used. Wild-type data corresponding to various concentrations of free $Ca^{2+}$ in the pipette solution (=[$Ca_f$]) were fitted with the biphasic Hill equation:

$$I_{MCU}/C_m = (I_{MCU}/C_m)_{\max}\left(1 - \frac{[Ca_f]^{H_{inh}}}{[Ca_f]^{H_{inh}} + {K_{inh}}^{H_{inh}}} \times \frac{{K_{rec}}^{H_{rec}}}{[Ca_f]^{H_{rec}} + {K_{rec}}^{H_{rec}}}\right),$$

where $H_{inh}$ and $H_{rec}$ are the Hill coefficients for inhibition and recovery from inhibition, respectively, while $K_{inh}$ and $K_{rec}$ are the correspondent mid-point pipette [$Ca_f$]. Least-square fitting was done with IGOR Pro software (WaveMetrics).

## Analysis of uniporter gatekeeping by simultaneous measurement of mitochondrial $Ca^{2+}$ uptake and mitochondrial membrane potential in permeabilized cells

Simultaneous measurement of mitochondrial $Ca^{2+}$ uptake and mitochondrial membrane potential ($\Delta\Psi_m$) in permeabilized HEK293 cells was performed as described (Mallilankaraman et al., 2012), with experimental data converted to and represented as bath $[Ca^{2+}]$. In brief, cells were trypsinized, counted and washed in a $Ca^{2+}$-free buffer, centrifuged and transferred to an intracellular-like medium (in mM: 120 KCl, 10 NaCl, 1 $KH_2PO_4$, 20 HEPES-Tris, 2 succinate, pH 7.2, protease inhibitors, 2 μM thapsigargin, 40 μg/ml digitonin) in a spectrofluorometer. FuraFF (0.5 μM) was added at 0 s and JC-1 (800 nM) at 20 s to measure extra-$[Ca^{2+}]_m$ and $\Delta\Psi_m$ at 37°C. Fluorescence was monitored in a

temperature-controlled (37°C) multi-wavelength-excitation dual wavelength-emission spectrofluorometer (Delta RAM, Photon Technology International) using 490-nm excitation/535-nm emission for the monomer, 570-nm excitation/595-nm emission for the J-aggregate of JC1and 340-nm/380-nm for FuraFF. In this study, the size of the $Ca^{2+}$ boluses added to stimulate subsequent mitochondrial $Ca^{2+}$ uptake did not change $\Delta\Psi_m$.

## Qualitative measurement of basal $[Ca^{2+}]_m$

Qualitative measurement of basal $[Ca^{2+}]_m$ were determined as we previously described (Mallilankaraman et al., 2012). Briefly, cells ($5\times10^5$/well) grown on 0.2% gelatin-coated coverslips in six-well dishes were loaded with 2 μM rhod-2 AM for 50 min in extracellular medium containing 2 mM $Ca^{2+}$. Coverslips were mounted in an open perfusion microincubator (PDMI-2; Harvard Apparatus) and imaged at 37 °C. All confocal images, obtained at 561 nm excitation using a 63× oil objective, were rapid 100 msec “snapshots” to avoid phototoxicity. All imaging used identical gain and exposure settings that enabled threshold detection of basal Rhod-2 fluorescence in control WT cells. Accordingly, the contribution of low-level diffuse background cytoplasmic Rhod-2 was essentially eliminated. Addition of the mitochondrial uncoupler CCCP (2–10 μM) was added to ensure that punctate fluorescence emanated from mitochondria (Figure S4). Images were analyzed using ImageJ software (NIH) as described (Mallilankaraman et al., 2012).

## Topology analysis

Topology analyses of MICU1, MICU2 and EMRE were performed by proteinase K protection assay as described (Sato et al., 1998). Mitochondria were isolated by differential centrifugation as described (Sato et al., 1998). Immediately after isolation, the mitochondrial pellet was resuspended in MIM buffer (280 mM sucrose with 10 mM Hepes; pH 7.2). Mitochondria (40 μg per condition) were placed in MIM buffer containing varying concentrations of digitonin (0–2%) and constant concentration of Proteinase-K (100 μg/ml) for 15 min at room temperature. Samples without proteinase-K or with 1% Triton X-100 served as controls. Proteinase-K was inactivated by addition of 10 μM PMSF, and samples were subjected to Western or dot blotting.

## Western blotting

Cells kept on ice were lysed with 1x RIPA lysis buffer (Millipore) supplemented with protease inhibitors (Complete, Roche). Membranes were blocked in 5% fat-free milk 1 hr at RT, incubated O/N at 4 °C with primary antibody, and then for 2 hr at RT with a secondary antibody conjugated to horseradish peroxidase (HRP). Chemiluminescence detection used ECL-plus reagent (Pierce). To ensure equal protein loading across gels, membranes were stripped (Restore western blot stripping buffer; Pierce) and re-probed with a loading control antibody. For dot blots, protein samples were spotted onto nitrocellulose membranes using a slot blot apparatus and immunoblotting was performed as described above. Antibodies for: MICU1 (ab102830, abcam; 1:200) and (HPA037480, Sigma; 1:300); MICU2 (ab101465, abcam 1:500) and (HPA045511; Sigma); MCU (HPA016480, Sigma; 1:500); EMRE (sc-86337; Santacruz) and (HPA032117, Sigma; 1:200); Tom20 (ab56783; abcam); Tim23 (611223; BD Biosciences); Tim44 (ab168649; abcam); Oxa1L (66128-1-Ig; proteintech); HSP60 (ab13532; abcam); anti-V5 (R960-25, Life technologies; 1:1000); anti-actin (A2228,

Sigma 1:2000); anti-flag (TA 50011, Origene 1:500); anti-mouse IgG-HRP (7076S, Cell Signaling; 1:1000) and anti-rabbit IgG-HRP (7074S, Cell Signaling; 1:1000) were used in the study. All experiments were done in triplicate.

### Co-immunoprecipitation

HEK293 cells (EMRE KO, EMRE KO + QN6 EMRE-V5 and EMRE KO + wild-type EMRE-V5) were grown to confluency in 150 mm plates. Cells were washed twice with PBS and lysed with 1 ml cold lysis buffer (50 mM HEPES-KOH pH 7.4, 150 mM NaCl, 0.2% n-dodecyl-β-D-maltoside, 0.5 mM EGTA, 0.3 mM $CaCl_2$, one Complete protease inhibitor tablet (Roche) per 30 ml lysis buffer). Cells were lysed at 4°C for 30 min and centrifuged at 16,000 × g. Cleared lysates were diluted to normalize for protein concentration. Appropriate volumes of lysates were added, corrected for expression levels based on western blotting and densitometric analysis. Anti-V5 Agarose (30 μl; Sigma #A 7345) was added to diluted lysates and rocked 16 hr at 4°C. Beads were washed with 1 ml PBS 3x and boiled in 90 μl 2x SDS sample buffer. 20 μl of each immunoprecipitate and 30 μg of total cell lysates were loaded on Tris-Glycine gels for Western Blotting. To maintain a constant range [$Ca^{2+}$] in lysis and wash buffers, $CaCl_2$ and EGTA were added to buffers according to http://maxchelatorStanford.edu/CaEGTA-TS.htm. In addition, [$Ca^{2+}$] in each preparation was measured with Fura-2. Solutions contained 150–450 nM free $Ca^{2+}$.

## Supplementary Material

Refer to Web version on PubMed Central for supplementary material.

## Acknowledgments

This work was supported by NIH GM56328 to J.K.F. We thank Dr. V. Mootha for knockout cell lines, and Dr. T. Hoshi for use of a spectrofluorometer. We also thank Drs. F. Fieni and Y. Kirichok for advice and training in mitoplast electrophysiology.

## References

Boyman L, Chikando AC, Williams GS, Khairallah RJ, Kettlewell S, Ward CW, Smith GL, Kao JP, Lederer WJ. Calcium movement in cardiac mitochondria. Biophys J. 2014; 107:1289–1301. [PubMed: 25229137]

Bragadin M, Pozzan T, Azzone GF. Kinetics of $Ca^{2+}$ carrier in rat liver mitochondria. Biochemistry. 1979; 18:5972–5978. [PubMed: 42437]

Brandenburger Y, Kennedy ED, Python CP, Rossier MF, Vallotton MB, Wollheim CB, Capponi AM. Possible role for mitochondrial calcium in angiotensin II- and potassium-stimulated steroidogenesis in bovine adrenal glomerulosa cells. Endocrinology. 1996; 137:5544–5551. [PubMed: 8940382]

Cardenas C, Miller RA, Smith I, Bui T, Molgo J, Muller M, Vais H, Cheung KH, Yang J, Parker I, et al. Essential regulation of cell bioenergetics by constitutive InsP3 receptor Ca2+ transfer to mitochondria. Cell. 2010; 142:270–283. [PubMed: 20655468]

Christel C, Lee A. $Ca^{2+}$-dependent modulation of voltage-gated $Ca^{2+}$ channels. Biochim Biophys Acta. 2012; 1820:1243–1252. [PubMed: 22223119]

Csordas G, Golenar T, Seifert EL, Kamer KJ, Sancak Y, Perocchi F, Moffat C, Weaver D, de la Fuente Perez S, Bogorad R, et al. MICU1 controls both the threshold and cooperative activation of the mitochondrial $Ca^{2+}$ uniporter. Cell metabolism. 2013; 17:976–987. [PubMed: 23747253]

De Stefani D, Rizzuto R. Molecular control of mitochondrial calcium uptake. Biochem Biophys Res Commun. 2014; 449:373–376. [PubMed: 24792182]

Fieni F, Lee SB, Jan YN, Kirichok Y. Activity of the mitochondrial calcium uniporter varies greatly between tissues. Nature communications. 2012; 3:1317.

Foskett JK, Madesh M. Regulation of mitochondrial $Ca^{2+}$ uniporter by MICU1 and MICU2. Biochemical and Biophysical Research Communications. 2014; 449:377–383. [PubMed: 24792178]

Foskett JK, Philipson B. The mitochondrial $Ca^{2+}$ uniporter complex. J Mol Cell Cardiol. 2015; 78:3–8. [PubMed: 25463276]

Gunter TE, Gunter KK, Sheu SS, Gavin CE. Mitochondrial calcium transport: physiological and pathological relevance. Am J Physiol. 1994; 267:C313–339. [PubMed: 8074170]

Gunter TE, Pfeiffer DR. Mechanisms by which mitochondria transport calcium. Am J Physiol. 1990; 258:C755–786. [PubMed: 2185657]

Ivannikov MV, Macleod GT. Mitochondrial free $Ca^{2+}$ levels and their effects on energy metabolism in Drosophila motor nerve terminals. Biophys J. 2013; 104:2353–2361. [PubMed: 23746507]

Kamer KJ, Mootha VK. MICU1 and MICU2 play nonredundant roles in the regulation of the mitochondrial calcium uniporter. EMBO Rep. 2014; 15:299–307. [PubMed: 24503055]

Kamer KJ, Sancak Y, Mootha VK. The uniporter: from newly identified parts to function. Biochem Biophys Res Commun. 2014; 449:370–372. [PubMed: 24814702]

Kirichok Y, Krapivinsky G, Clapham DE. The mitochondrial calcium uniporter is a highly selective ion channel. Nature. 2004; 427:360–364. [PubMed: 14737170]

Lam SS, Martell JD, Kamer KJ, Deerinck TJ, Ellisman MH, Mootha VK, Ting AY. Directed evolution of APEX2 for electron microscopy and proximity labeling. Nat Methods. 2015; 12:51–54. [PubMed: 25419960]

Logan CV, Szabadkai G, Sharpe JA, Parry DA, Torelli S, Childs AM, Kriek M, Phadke R, Johnson CA, Roberts NY, et al. Loss-of-function mutations in MICU1 cause a brain and muscle disorder linked to primary alterations in mitochondrial calcium signaling. Nat Genet. 2014; 46:188–193. [PubMed: 24336167]

Lukacs GL, Kapus A. Measurement of the matrix free $Ca^{2+}$ concentration in heart mitochondria by entrapped fura-2 and quin2. Biochem J. 1987; 248:609–613. [PubMed: 3435469]

Mallilankaraman K, Doonan P, Cardenas C, Chandramoorthy HC, Muller M, Miller R, Hoffman NE, Gandhirajan RK, Molgo J, Birnbaum MJ, et al. MICU1 is an essential gatekeeper for MCU-mediated mitochondrial $Ca^{2+}$ uptake that regulates cell survival. Cell. 2012; 151:630–644. [PubMed: 23101630]

Nicholls DG. Mitochondrial calcium function and dysfunction in the central nervous system. Biochim Biophys Acta. 2009; 1787:1416–1424. [PubMed: 19298790]

Palmer AE, Giacomello M, Kortemme T, Hires SA, Lev-Ram V, Baker D, Tsien RY. $Ca^{2+}$ indicators based on computationally redesigned calmodulin-peptide pairs. Chem Biol. 2006; 13:521–530. [PubMed: 16720273]

Patron M, Checchetto V, Raffaello A, Teardo E, Vecellio Reane D, Mantoan M, Granatiero V, Szabo I, De Stefani D, Rizzuto R. MICU1 and MICU2 finely tune the mitochondrial $Ca^{2+}$ uniporter by exerting opposite effects on MCU activity. Mol Cell. 2014; 53:726–737. [PubMed: 24560927]

Perocchi F, Gohil VM, Girgis HS, Bao XR, McCombs JE, Palmer AE, Mootha VK. MICU1 encodes a mitochondrial EF hand protein required for $Ca^{2+}$ uptake. Nature. 2010; 467:291–296. [PubMed: 20693986]

Petrungaro C, Zimmermann KM, Kuttner V, Fischer M, Dengjel J, Bogeski I, Riemer J. The $Ca^{2+}$-dependent release of the Mia40-induced MICU1-MICU2 dimer from MCU regulates mitochondrial $Ca^{2+}$ uptake. Cell metabolism. 2015; 22:721–733. [PubMed: 26387864]

Sancak Y, Markhard AL, Kitami T, Kovacs-Bogdan E, Kamer KJ, Udeshi ND, Carr SA, Chaudhuri D, Clapham DE, Li AA, et al. EMRE is an essential component of the mitochondrial calcium uniporter complex. Science. 2013; 342:1379–1382. [PubMed: 24231807]

Sato T, Mihara K. Mammalian Oxa1 protein is useful for assessment of submitochondrial protein localization and mitochondrial membrane integrity. Anal Biochem. 2010; 397:250–252. [PubMed: 19854151]

Sato Y, Miyazaki S, Shikano T, Mitsuhashi N, Takeuchi H, Mikoshiba K, Kuwabara Y. Adenophostin, a potent agonist of the inositol 1,4,5-trisphosphate receptor, is useful for fertilization of mouse

oocytes injected with round spermatids leading to normal offspring. Biol Reprod. 1998; 58:867–873. [PubMed: 9510978]

Vais H, Tanis JE, Muller M, Payne R, Mallilankaraman K, Foskett JK. MCUR1, CCDC90A, Is a Regulator of the Mitochondrial Calcium Uniporter. Cell metabolism. 2015; 22:533–535. [PubMed: 26445506]

Zoccarato F, Nicholls D. The role of phosphate in the regulation of the independent calcium-efflux pathway of liver mitochondria. European journal of biochemistry/FEBS. 1982; 127:333–338. [PubMed: 6183118]

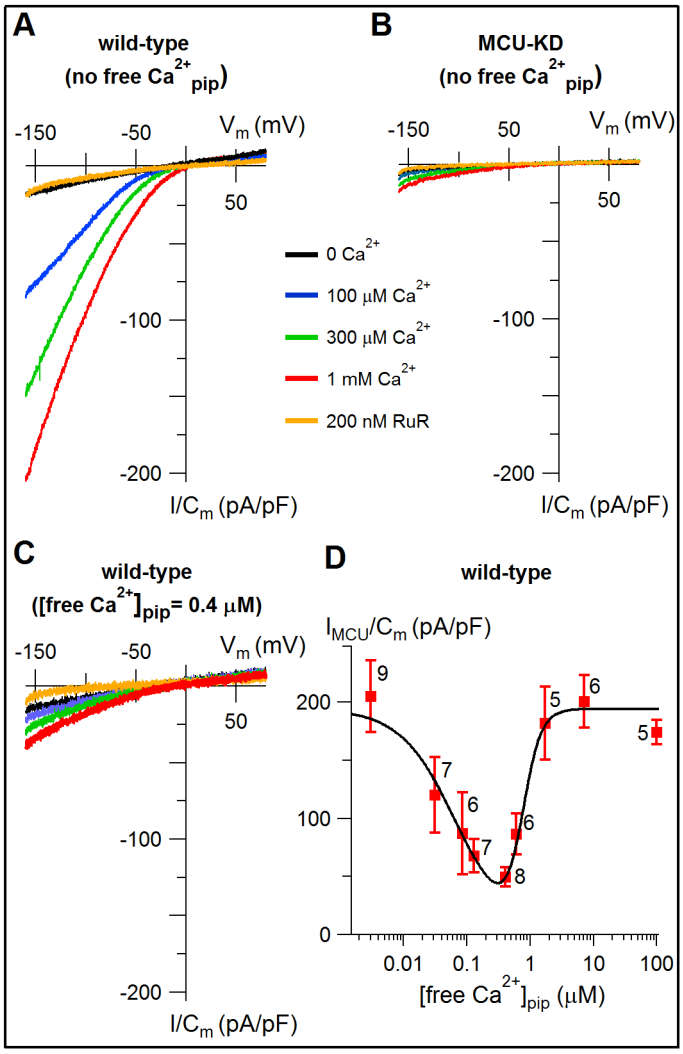


**Figure 1. MCU channel activity is modulated by a mechanism dependent upon matrix [$Ca^{2+}$]**

(A) MCU current density in various bath [$Ca^{2+}$] (indicated in inset) with 0 $Ca^{2+}$ (1.5 mM EGTA) in the pipette solution, in response to voltage ramps from −160 to 60 mV. Inhibition by ruthenium red (RuR, 200 nM) in 1 mM bath $Ca^{2+}$ also shown.

(B) MCU current density measured from MCU-KD cells.

(C) Similar to panel (A), recorded with pipette solution containing 400 nM free $Ca^{2+}$.

(D) Response of MCU $Ca^{2+}$current density at $V_m$ = −160 mV, with 1 mM $Ca^{2+}$ in the bath, as function of free [$Ca^{2+}$] in pipette (matrix) solution. Data fitted with a biphasic Hill equation (continuous line).

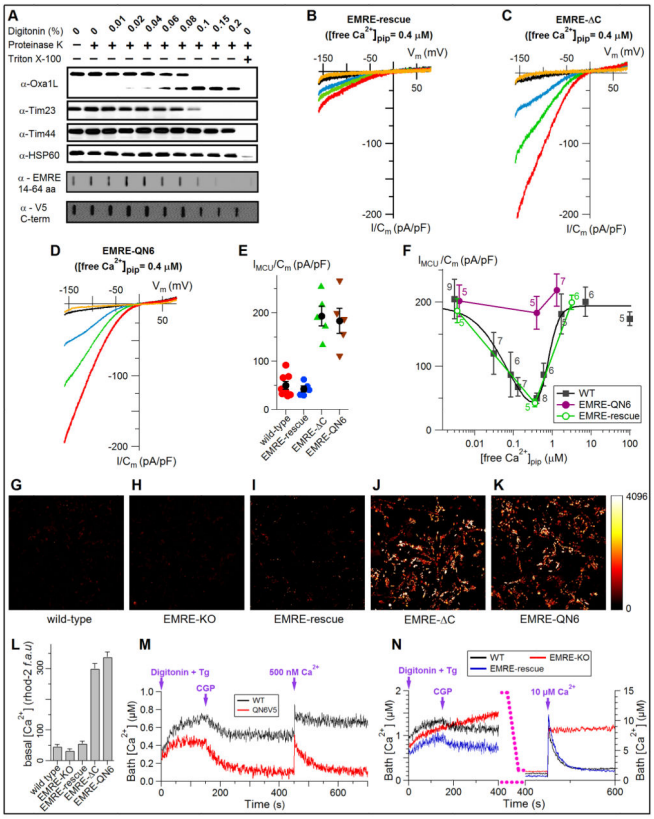


**Figure 2. The carboxyl terminus of EMRE confers matrix [$Ca^{2+}$] sensitivity to MCU activity**

(A) The carboxyl terminus of EMRE resides in the matrix. EMRE-rescue (V5-tagged EMRE over-expressed in EMRE-KO cells) was probed for its amino- (α-EMRE) and carboxyl (α-V5) termini. Carboxyl terminus is protected from protease similarly to matrix-localized proteins.

(B to D) MCU current densities in various bath [$Ca^{2+}$], recorded from mitoplasts from EMRE KO cells expressing wild-type EMRE (B), EMRE-ΔC (C) or EMRE-QN6 (D), with pipette solution containing 400 nM free $Ca^{2+}$. Color schemes as in Figure 1.

(E) Summary of experiments shown in B–D. Means and SEMs. Wild-type (Figure 1D) and EMRE-rescue data included for comparison.

(F) Response of MCU $Ca^{2+}$current density at $V_m$ = −160 mV, with 1 mM $Ca^{2+}$ in the bath, as function of free [$Ca^{2+}$] in pipette (matrix) solution for indicated cells, showing loss of matrix [Ca2+] regulation in mitoplasts expressing EMRE-QN6. Wild-type data fitted with a biphasic Hill equation (continuous line).

(G to K) Basal Rhod-2 fluorescence in cells stably expressing EMRE constructs.

(L) Rhod-2 fluorescence quantification (fluorescence arbitrary units (f.a.u.); Mean ± SEM, n = 3).

(M) Gatekeeping measured by mitochondrial $Ca^{2+}$ uptake (average traces; n = 3) in permeabilized cells is abolished in cells expressing the EMRE-QN6 mutant, evidenced by MCU-mediated $Ca^{2+}$ uptake following inhibition of the $Na^+/Ca^{2+}$ exchanger with CGP that reduces baseline bath [$Ca^{2+}$] to much lower levels than wild-type (WT) cells, and their

ability to rapidly take up $Ca^{2+}$ following addition of 500 nM $Ca^{2+}$ bolus. Tg: thapsigargin, 2 μM. Digitonin: 40 μg/ml. See text for details.

(N) Similar to (M), demonstrating lack of MCU activity in EMRE KO cells (no $Ca^{2+}$ uptake following CGP addition or after addition of 10 μM $Ca^{2+}$ bolus) and normal gatekeeping and $Ca^{2+}$ uptake in WT and EMRE-rescue cells.

See also Figures S1 to S4.

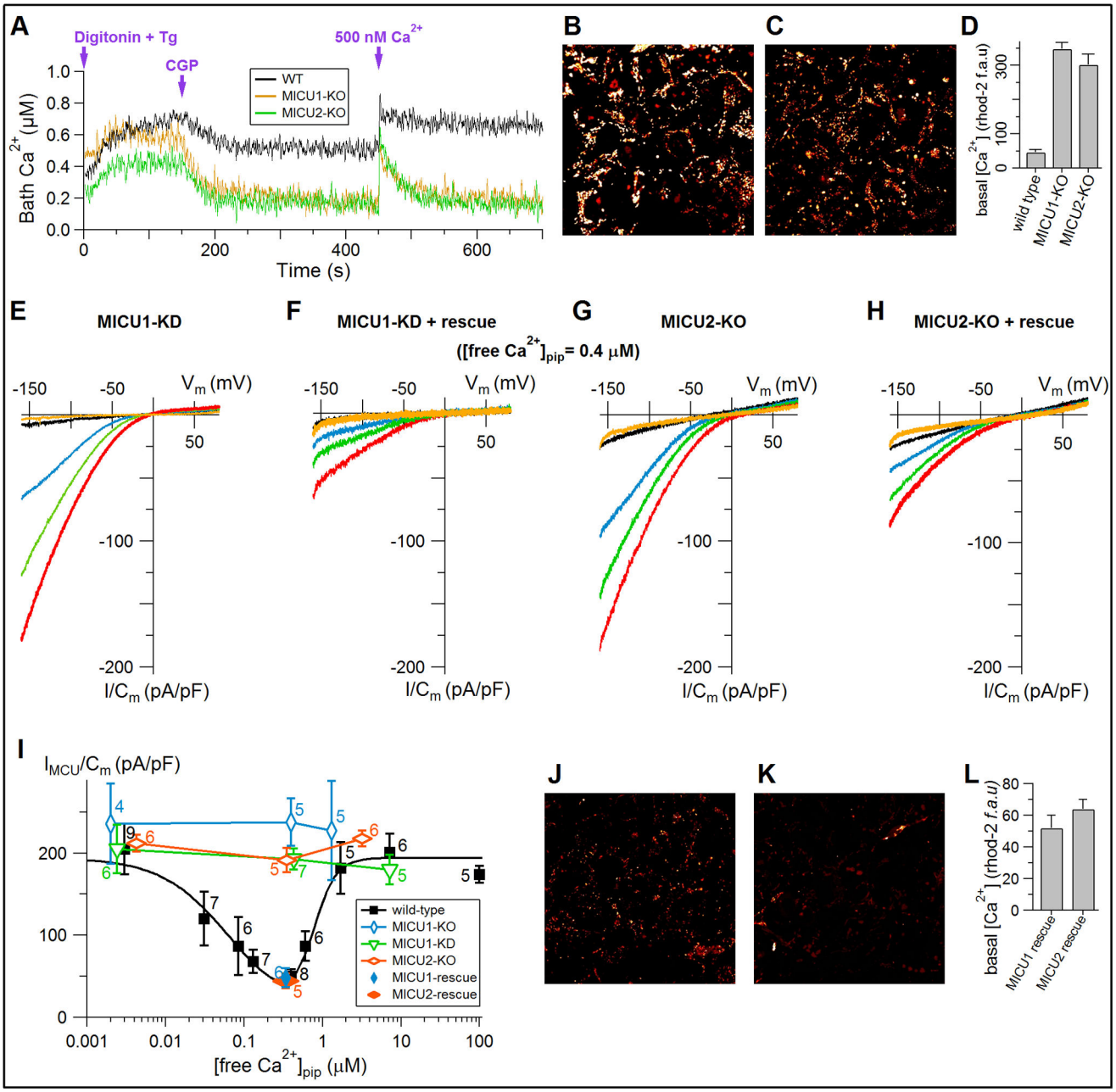


**Figure 3. MICU1 and MICU2 are required for matrix [$Ca^{2+}$] regulation of MCU**

(A) Average traces (n = 3) of bath [$Ca^{2+}$] showing inhibition of gatekeeping in MICU1-KO and MICU2-KO cells as evidenced by MCU-mediated $Ca^{2+}$ uptake that reduces baseline bath [$Ca^{2+}$] to much lower levels than wild-type (WT) cells, and ability of KO cells to rapidly take up $Ca^{2+}$ following addition of 500 nM $Ca^{2+}$ bolus.

(B and C) Basal Rhod-2 fluorescence in MICU1-KO (B) and MICU2-KO (C) cells.

(D) Quantification of Rhod-2 fluorescence (mean ± SEM, n = 3).

(E and F) Representative MCU currents in various bath [$Ca^{2+}$] from mitoplasts from MICU1-KD (E) or MICU1-rescue (F) cells, with pipette solution containing 400 nM free $Ca^{2+}$. Color scheme as in Fig. 1.

(G and H) Representative MCU currents in various bath [$Ca^{2+}$] recorded from MICU2-KO (G) or MICU2 rescue (H) mitoplasts, with pipette solution containing 400 nM free $Ca^{2+}$. Color scheme as in Fig. 1.

(I) Summary of MCU current densities over range of matrix [$Ca^{2+}$] in mitoplasts from wild-type (WT) and MICU1 and MICU2 KD/KO and rescue cells.

(J and K) Basal Rhod-2 fluorescence in MICU1 (J) and MICU2 (K) rescue cells.

(L) Quantification of Rhod-2 fluorescence (mean ± SEM, n = 3).

See also Figure S2 and S4.

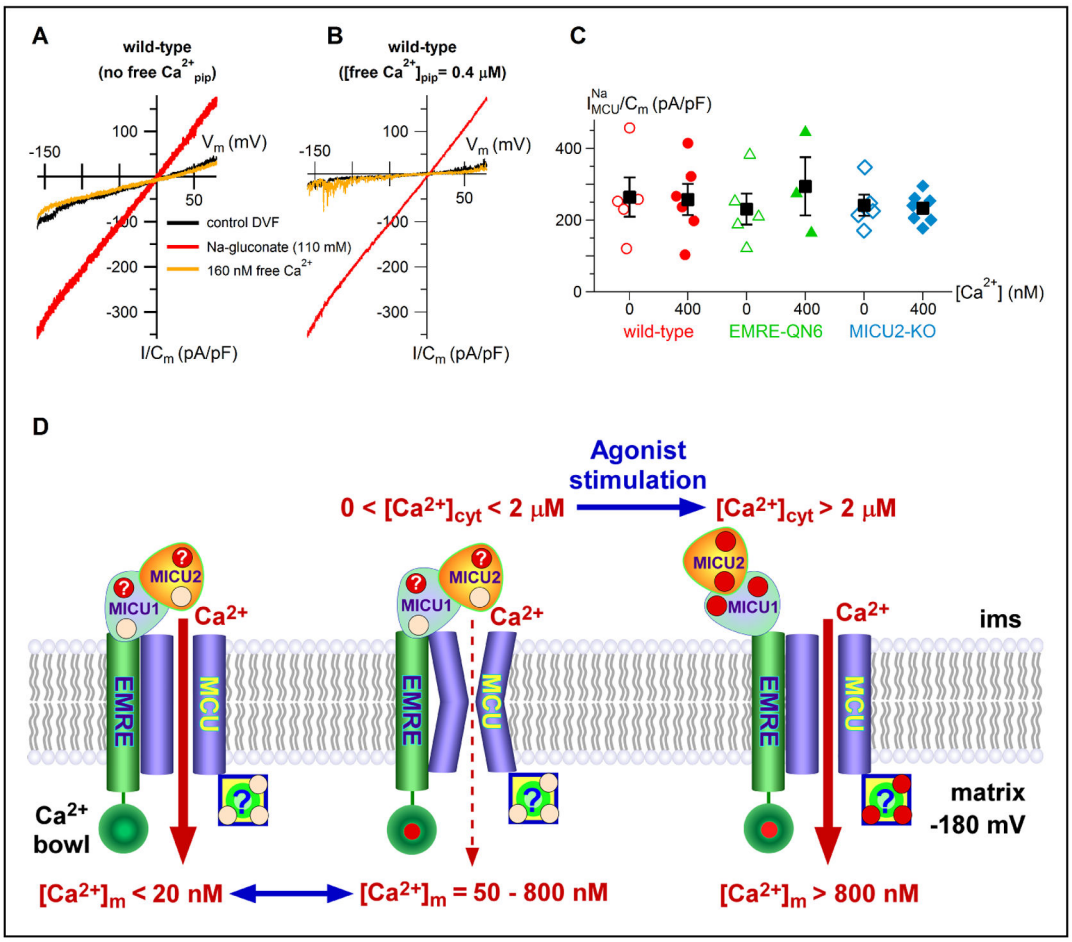


**Figure 4. Matrix [$Ca^{2+}$] regulation of MCU requires cytoplasmic $Ca^{2+}$**

(A) Representative MCU-mediated $Na^+$ currents (red trace) recorded in absence of bath $Ca^{2+}$ with no free $Ca^{2+}$ in pipette. Addition of 160 nM free $Ca^{2+}$ to bath completely blocked the $Na^+$ current (orange trace).

(B) Same as in (A), recorded with pipette solution containing 400 nM free $Ca^{2+}$.

(C) Summary of MCU $Na^+$ current densities in different cell types with pipette solutions with or without 400 nM free $Ca^{2+}$.

(D) Model for MCU regulation, with $Ca^{2+}$ sensors on both sides of the IMM: EMRE and an unknown protein (box associated with MCU in the cartoon) sense matrix [$Ca^{2+}$] ($[Ca^{2+}]_m$); MICU1 and/or MICU2, through their paired EF hands (red dots), represent intermembrane space (ims) cytoplasmic $Ca^{2+}$ ($[Ca^{2+}]_{cyt}$) sensor(s). Under normal resting conditions (middle conformation), channel open probability is strongly reduced (gatekeeping) when sensors on both sides of the IMM are liganded with $Ca^{2+}$ (red dots with question marks signify $Ca^{2+}$ binding sites possibly liganded). Channel inhibition is effective in the range of $[Ca^{2+}]_m$ = 50–800 nM, with maximal inhibition at $[Ca^{2+}]_m$ ~ 400 nM (from $I_{MiCa}$ biphasic matrix [$Ca^{2+}$] dependence with apparent inhibition constant of 60 nM and apparent recovery constant of 730 nM; Figure 1D) with peak inhibition of MCU currents by ~75% at ~400 nM (25% open probability indicated by dashed line in middle conformation)), and $[Ca^{2+}]_{cyt}$ between resting levels and ~ 2 µM (from permeabilized cell measurements here and in

(Mallilankaraman et al., 2012). Physiological relief of MCU channel inhibition is achieved by agonist-induced elevated $[Ca^{2+}]_{cyt}$ that drives $Ca^{2+}$ into the matrix, raising $[Ca^{2+}]_m$ to levels (>800 nM) that result in highly cooperative activation (Hill coefficient > 3) of mitochondrial $Ca^{2+}$ influx by unknown mechanisms (right conformation, with the unknown matrix reactivation mechanism(s) depicted as a $Ca^{2+}$ binding protein with multiple $Ca^{2+}$ binding sites, and MICU proteins with EF hands fully liganded). MCU channel inhibition can also be relieved by very low $[Ca^{2+}]_m$ (left conformation) as a result of $Ca^{2+}$ unbinding from EMRE, independent of the $Ca^{2+}$ binding states of MICU proteins (See also Figure S4B).